Supplementary Information

Low lattice thermal conductivity induced by rattling-like vibration in RbCaX (X = As, Sb) compounds with excellent thermoelectric properties

JingYi Zhang,‡[a] Junhao Peng,‡[a] Runqing Zhang,[a] Yanwei Liang,[a] Zihan Xu,[a] Renhai Wang,[a] Fugen Wu,*[b] Da Wan,[c] Pengfei Zhang,[c] Shulin Bai,[c] Huafeng Dong*[a]

[a]Guangdong Provincial Key Laboratory of Sensing Physics and System Integration Applications, School of Physics and Optoelectronic Engineering, Guangdong University of Technology, Guangzhou 510006, China

[b]The College of Information Engineering, Guangzhou Vocational University of Science and Technology, Guangzhou 510550, China

[c]College of Materials Science and Engineering, Liaoning Technical University, Fuxin, Liaoning 123000, China.

‡equal contribution

*Corresponding author E-mail: wufugen@gkd.edu.cn; hfdong@gdut.edu.cn

Contents

Section 1. Electronic properties and stability analysis

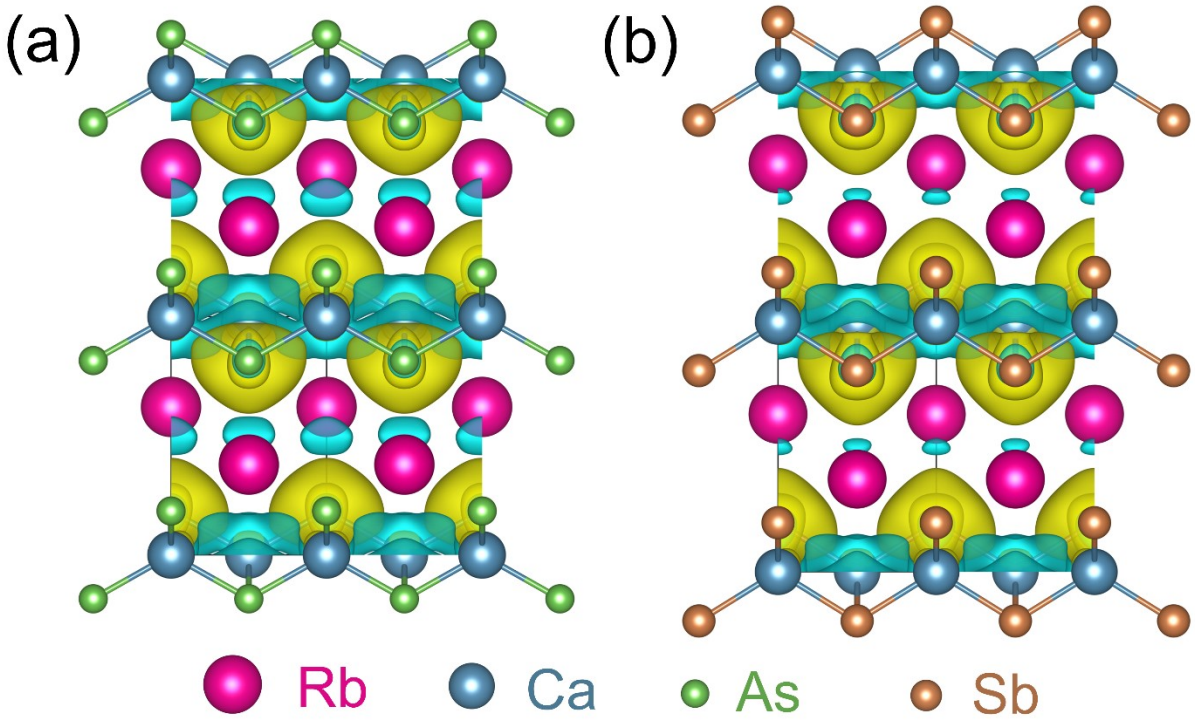

Fig. S1. Charge density difference diagram of (a) RbCaAs and (b) RbCaSb. The cyan region indicates charge loss and the yellow region indicates charge gain. The isosurface value is set to 0.0025 e/Å^3.

Table S1. Charge states (in |e|) of RbCaX (X = As, Sb) compounds based on Bader charge analysis.

System	Rb1	Rb2	Ca1	Ca2	As1/Sb1	As2/Sb2
RbCaAs	-0.68	-0.68	-1.28	-1.28	+1.96	+1.96
RbCaSb	-0.70	-0.70	-1.24	-1.24	+1.94	+1.94

First, the interaction strength can be qualitatively analyzed using the charge density difference ($\Delta\rho(r)$). Taking the RbCaAs as an example, $\Delta\rho(r)$ is defined as: $\Delta\rho(r) = \rho(\mathrm{RbCaAs}) - \rho(\mathrm{Rb}) - \rho(\mathrm{Ca}) - \rho(\mathrm{As})$ [1]. Here, $\Delta\rho(r)$ denotes the charge density of RbCaAs compound, while $\rho(\mathrm{Rb})$, $\rho(\mathrm{Ca})$ and $\rho(\mathrm{As})$ represent the charge densities of isolated, non-interacting Rb, Ca and As atoms, respectively, calculated at the same atomic positions and within the same supercell as in the compound. $\Delta\rho(r)$ defined in this way to characterize the charge redistribution caused by different interactions. The charge density differences of RbCaX (X = As, Sb) compounds are plotted in **Fig. S1**. A positive value (yellow area) in plot indicates an increase in electron density after bonding, and a negative value (cyan area) indicates a decrease in electron density. As can be seen

from **Fig. S1**, the charge density differences of RbCaAs and RbCaSb is primarily distributed around the Ca-As/Sb bonds, indicating strong intralayer interaction. In contrast, at an isosurface value of 0.0025 e/Å³, the region around Rb atoms exhibits only minor charge redistribution, suggesting weak interlayer interactions. Next, the charge transfer of the two compounds was quantitatively assessed using Bader charge analysis (see **Table S1**). The results show that in both RbCaAs and RbCaSb, the charge transfer from Ca to As/Sb atoms within the layer is approximately 1.28 and 1.24 electrons, respectively. This indicates significant intralayer electron transfer. In comparison, the interlayer charge transfer from Rb atoms is only half that of the intralayer charge transfer, further reinforcing that interlayer interactions are weak.

In summary, the RbCaX (X = As, Sb) compounds exhibit strong intralayer interactions and relatively weak interlayer interactions. This conclusion is supported by consistent evidence from geometric structure, electron density redistribution and charge transfer behavior.

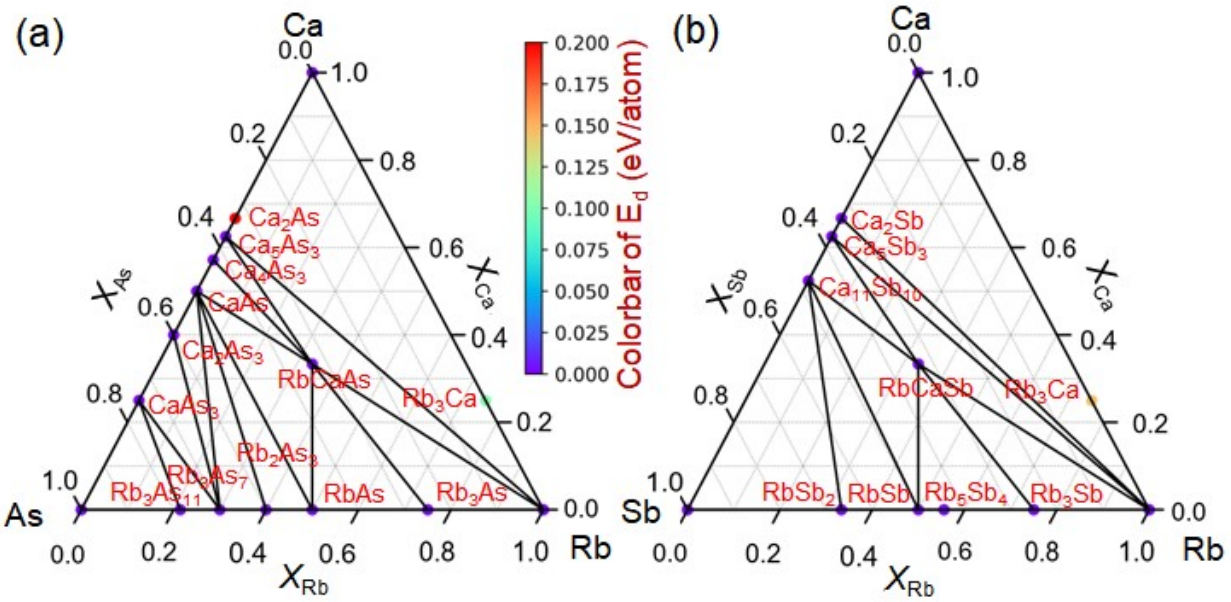

Fig. S2. The convex hull diagram of RbCaX (X = As, Sb) confirms its stability in the *P*4/*nmm* space group concerning other secondary phases. Various colours represent the scale of formation energy above the convex hull, indicated by the adjacent colour coding. The purple dots on the Gibbs triangles connected by black lines represent stable compounds, while the other points indicate metastable phases.

Table S2. The calculated elastic constant (C_{ij}, GPa) for RbCaX (X = As, Sb), along with the Bulk modulus (B_{VRH}, GPa), Shear modulus (G_{VRH}, GPa), Young's modulus (Y_{VRH}, GPa) and Poisson's ratio

(ν_{VRH}), ratio of bulk modulus to shear modulus (B_H/G_H), where VRH stands for the Voigt-Reuss-Hill approach.

System	C_{11}	C_{12}	C_{13}	C_{33}	C_{44}	C_{66}	B_{VRH}	G_{VRH}	Y_{VRH}	ν_{VRH}	B_H/G_H
RbCaAs	44.56	5.14	14.48	33.61	5.37	15.58	21.21	9.83	25.54	0.30	2.16
RbCaSb	34.87	4.15	12.41	29.49	5.04	11.83	17.45	8.26	21.40	0.30	2.11

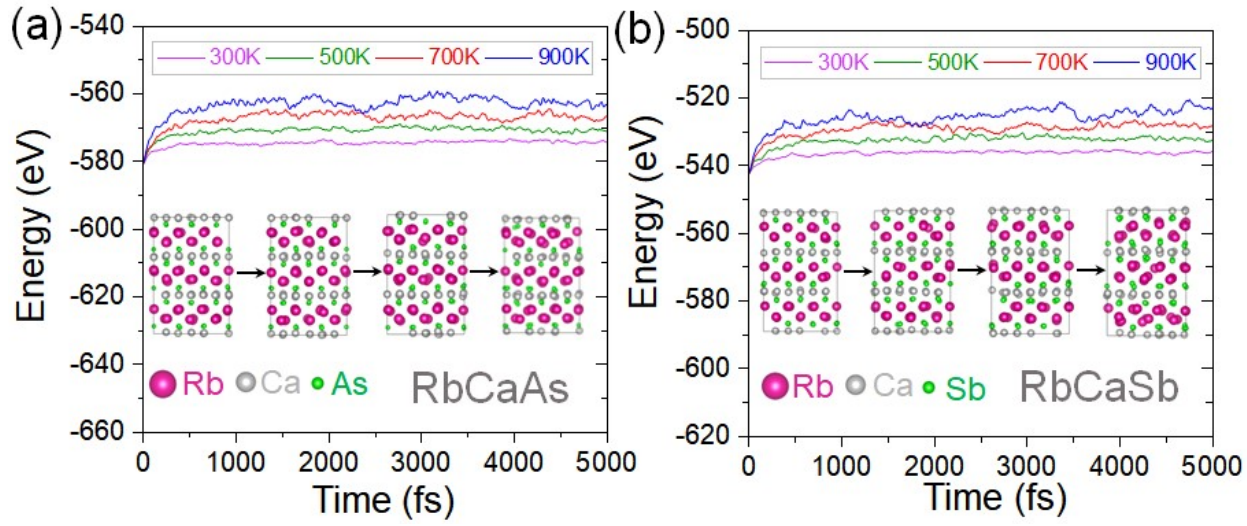

Fig. S3. Total energy fluctuations of (a) RbCaAs and (b) RbCaSb in AIMD simulations at 300, 500, 700, and 900 K. Insets show atomic structure snapshots at the end of the simulations.

Section 2. Electronic transport property calculations

2.1 AMSET settings

Table S3. The zero-weighted density of states (DOS), interpolated DOS, and finite-difference parameters used in AMSET for RbCaX (X = As, Sb) are presented. The high-frequency dielectric constant, ionic dielectric constant, elastic constants, piezoelectric constant (of 0) and polar optical phonon frequency were calculated using the finite-difference method, ensuring accurate evaluation of these properties. The static dielectric constant was obtained as the sum of the high-frequency and ionic dielectric constants.

Parameter	Zero-weighted DOS	Interpolated DOS	Finite-difference
k-point mesh	12×12×8	59×59×37	3×3×3

These are the input parameters for AMSET in RbCaX (X = As, Sb)

AMSET Parameters	RbCaAs	RbCaSb

Elastic constant tensor (GPa)	$\begin{pmatrix} 44.56 & 5.14 & 14.48 & 0 & 0 & 0 \\ 5.14 & 44.56 & 14.48 & 0 & 0 & 0 \\ 14.48 & 14.48 & 33.61 & 0 & 0 & 0 \\ 0 & 0 & 0 & 5.37 & 0 & 0 \\ 0 & 0 & 0 & 0 & 5.37 & 0 \\ 0 & 0 & 0 & 0 & 0 & 15.58 \end{pmatrix}$	$\begin{pmatrix} 34.87 & 4.15 & 12.41 & 0 & 0 & 0 \\ 4.15 & 34.87 & 12.41 & 0 & 0 & 0 \\ 12.41 & 12.41 & 29.49 & 0 & 0 & 0 \\ 0 & 0 & 0 & 5.04 & 0 & 0 \\ 0 & 0 & 0 & 0 & 5.04 & 0 \\ 0 & 0 & 0 & 0 & 0 & 11.83 \end{pmatrix}$
High-frequency dielectric constant tensor (ε0)	$\begin{pmatrix} 6.17 & 0 & 0 \\ 0 & 6.17 & 0 \\ 0 & 0 & 5.51 \end{pmatrix}$	$\begin{pmatrix} 6.44 & 0 & 0 \\ 0 & 6.44 & 0 \\ 0 & 0 & 5.65 \end{pmatrix}$
Static dielectric constant tensor (ε0)	$\begin{pmatrix} 14.88 & 0 & 0 \\ 0 & 14.88 & 0 \\ 0 & 0 & 9.03 \end{pmatrix}$	$\begin{pmatrix} 14.28 & 0 & 0 \\ 0 & 14.28 & 0 \\ 0 & 0 & 9.11 \end{pmatrix}$
Polar optical phonon frequency (THz)	3.79	3.25

2.2 Convergence tests for electron transport and thermoelectric properties calculations

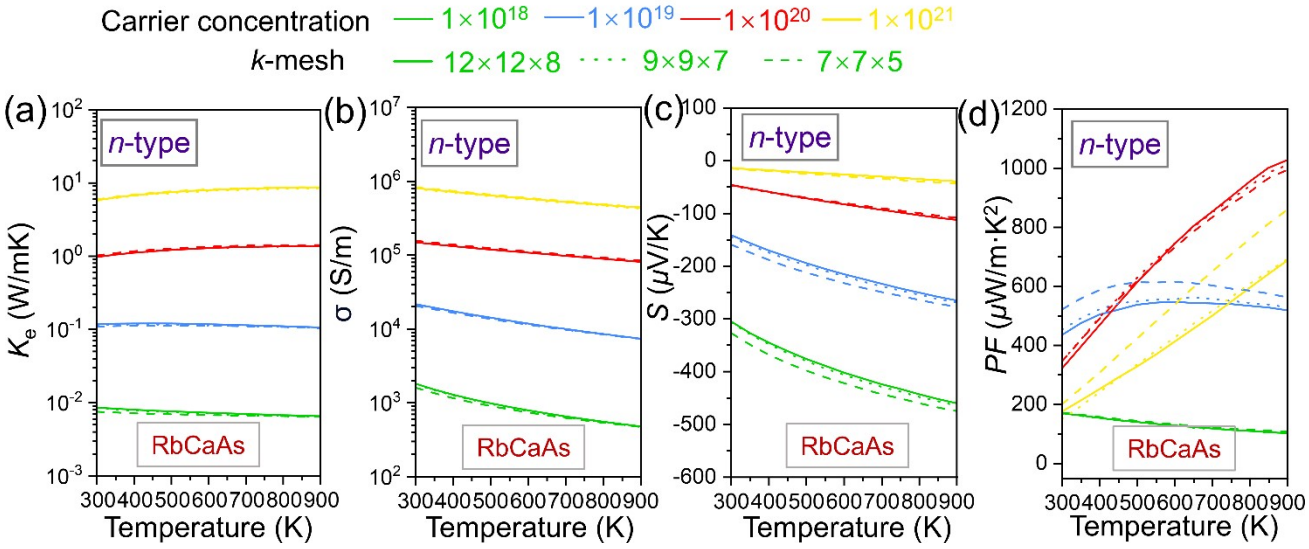

Fig. S4. Convergence test for calculated electron transport and thermoelectric properties of *n*-type RbCaAs structure. Calculations over different *k*-meshes with the interpolation factor fixed to 50.

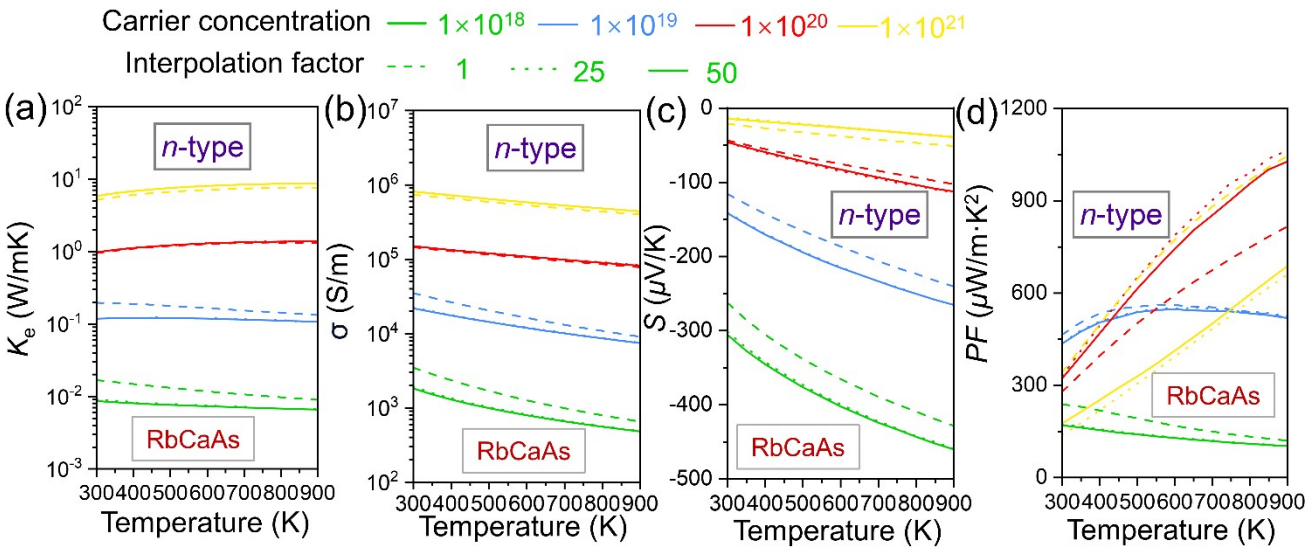

Fig. S5. Convergence test for calculated electron transport and thermoelectric properties of *n*-type RbCaAs structure. Calculations over different interpolation factors with *k*-mesh fixed to 12×12×8.

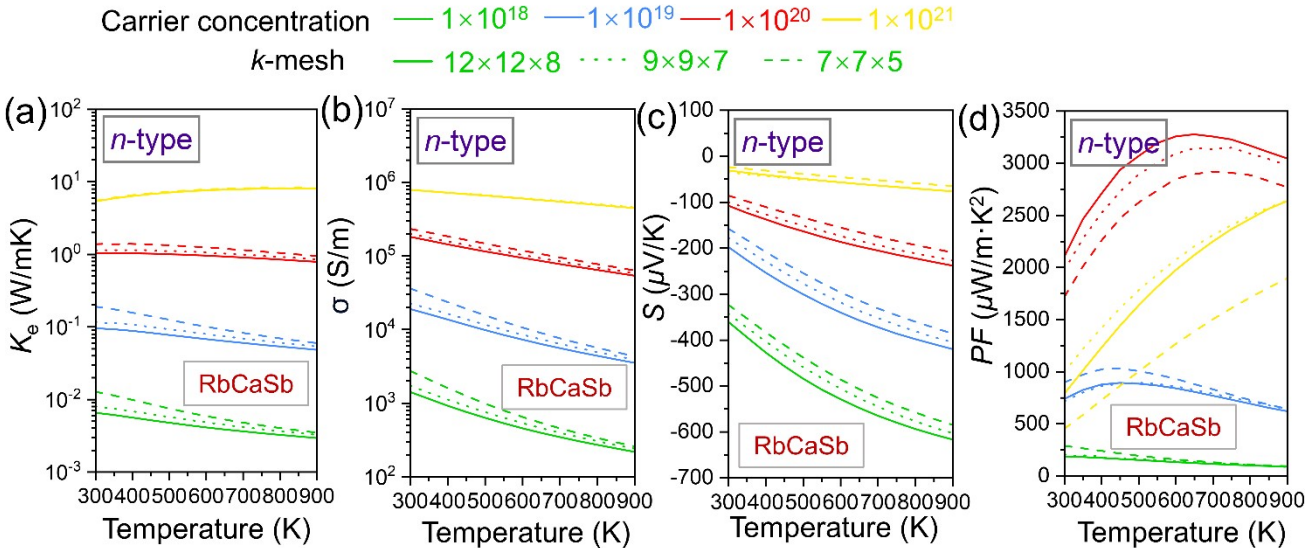

Fig. S6. Convergence test for calculated electron transport and thermoelectric properties of *n*-type RbCaSb structure. Calculations over different *k*-meshes with interpolation factor fixed to 50.

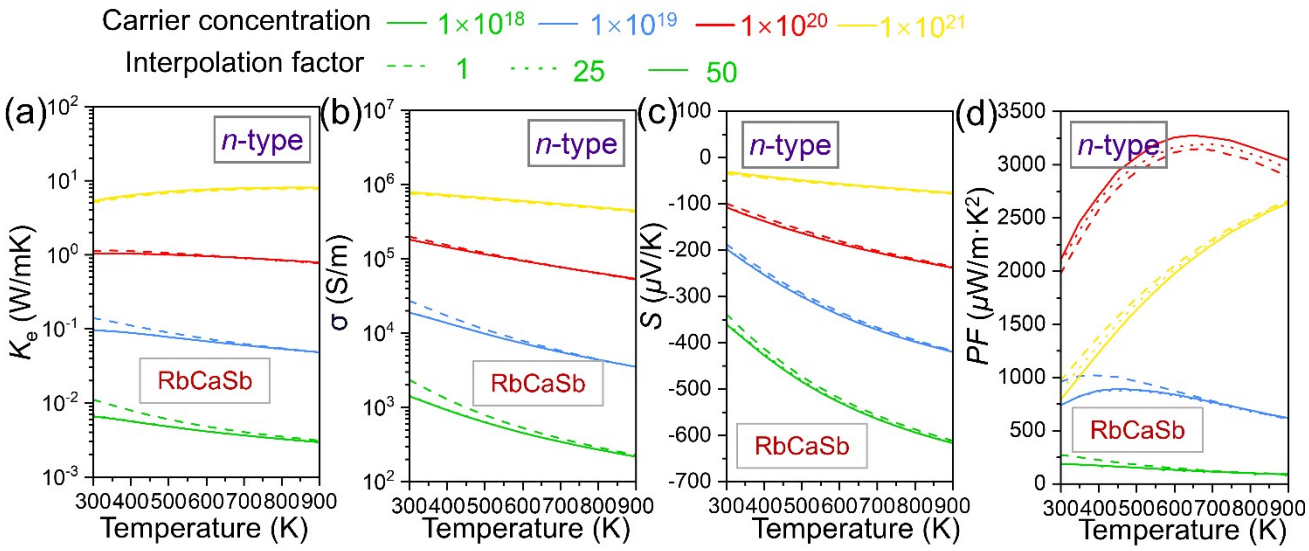

Fig. S7. Convergence test for calculated electron transport and thermoelectric properties of *n*-type RbCaSb structure. Calculations over different interpolation factors with *k*-mesh fixed to 12×12×8.

2.3 Electronic transport properties analysis

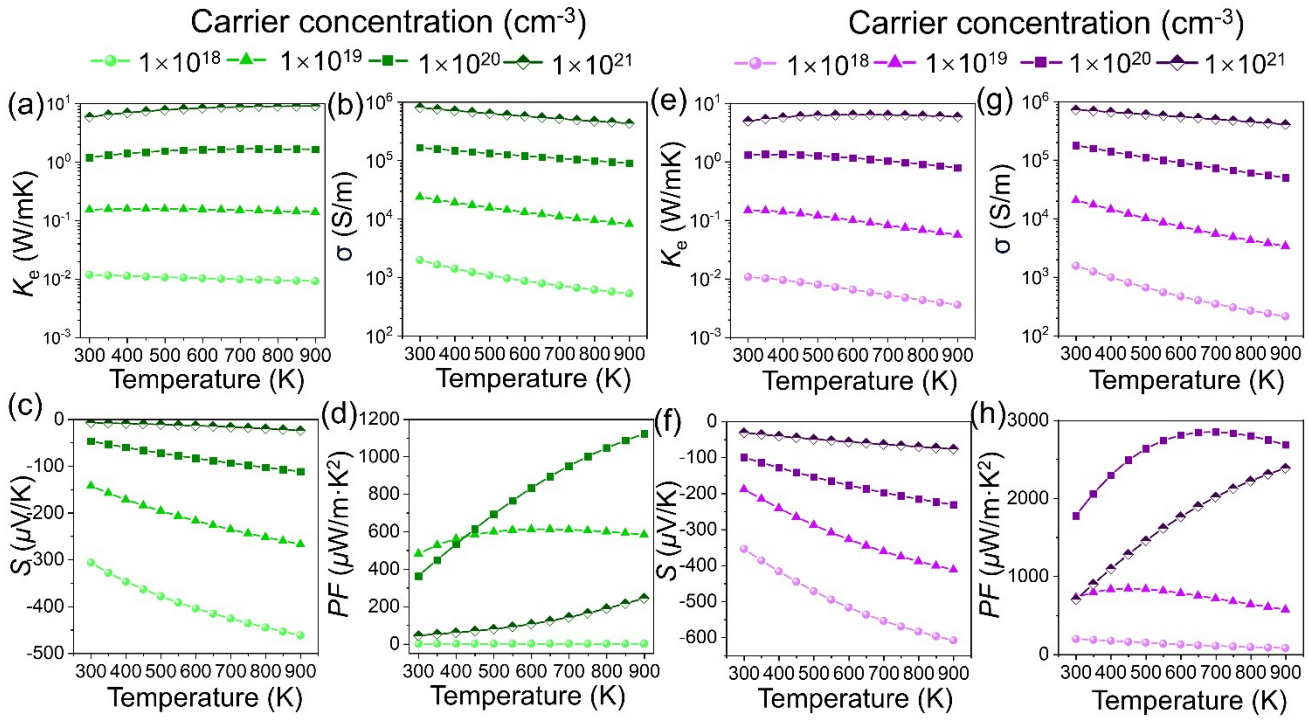

Fig. S8. Calculated electronic transport properties as a function of temperature for *n*-type (a-d) RbCaAs and (e-h) RbCaSb in the *xy* plane with four different carrier concentrations.

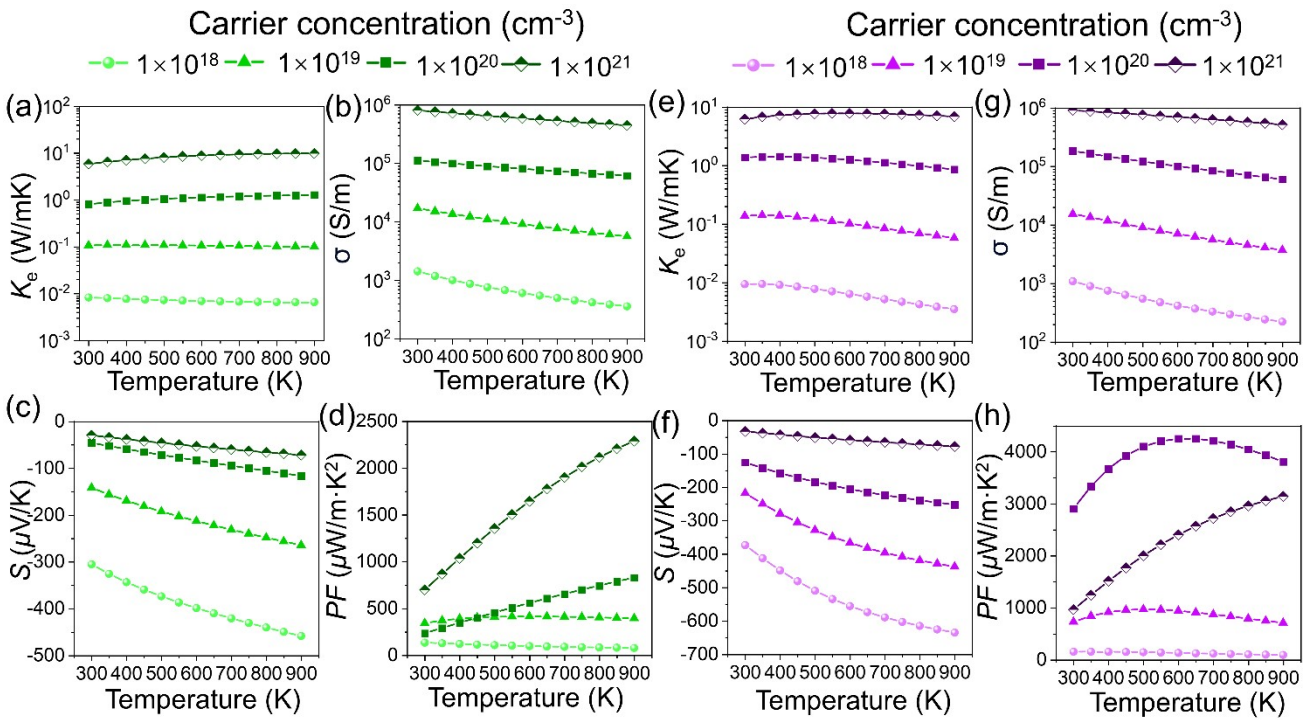

Fig. S9. Calculated electronic transport properties as a function of temperature for *n*-type (a-d) RbCaAs and (e-h) RbCaSb along the *z* direction with four different carrier concentrations.

Section 3. Phonon thermal transport properties analysis

3.1 Convergence tests of phonon dispersion calculation

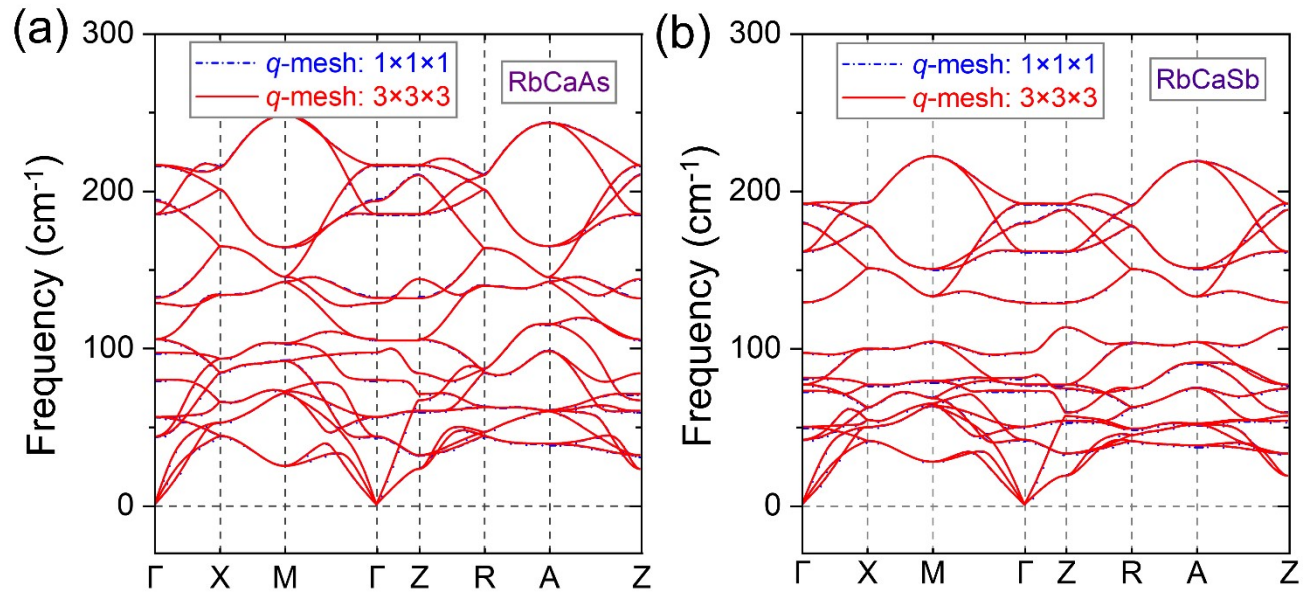

Fig. S10. The phonon spectra of (a) RbCaAs and (b) RbCaSb calculated using 3×3×3 supercell on 1×1×1 and 3×3×3 *q*-point meshes.

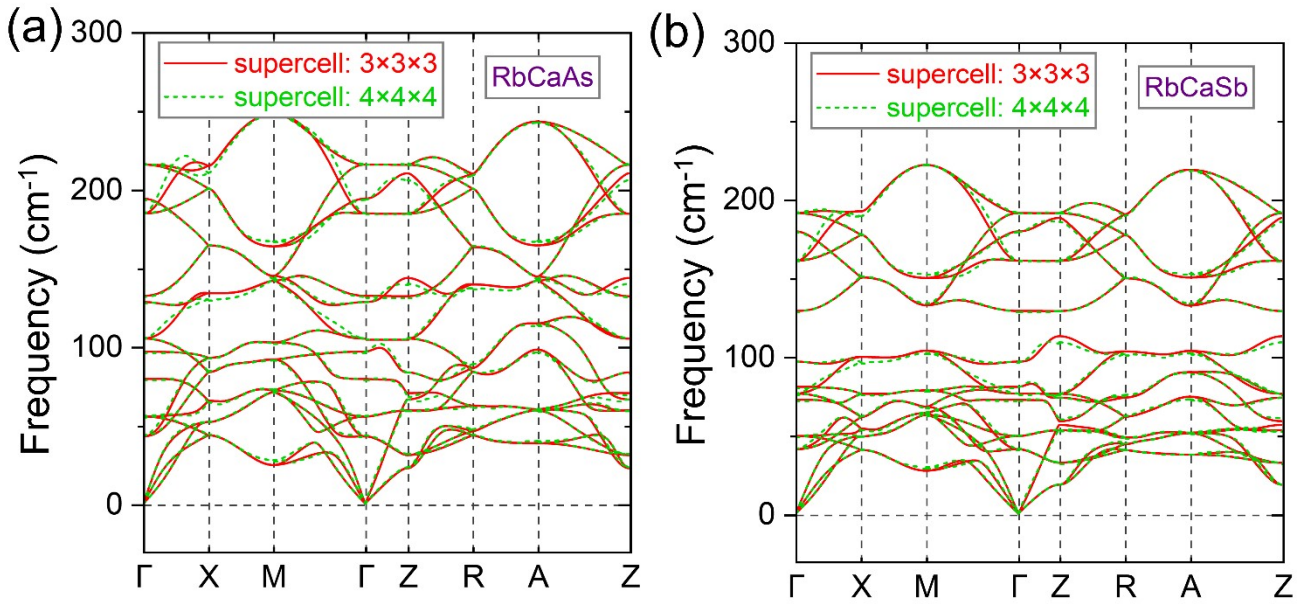

Fig. S11. The phonon spectra of (a) RbCaAs and (b) RbCaSb calculating using different supercell sizes, with a *q*-point mesh of 1×1×1.

Fig. S10 shows the phonon dispersion of RbCaX (X = As, Sb) using two different *q*-point meshes: 1×1×1 and 3×3×3. This comparison evaluates the convergence of the phonon dispersion calculations to ensure that the chosen *q*-point density accurately describes the phonon behavior. For two compounds, the phonon dispersion curves are nearly identical for both meshes. This suggests that the coarser 1×1×1 *q*-point mesh provides a reasonable approximation, while the finer 3×3×3 *q*-point mesh offers enhanced accuracy in resolving phonon modes. To maintain computational rigor, a 3×3×3 *q*-point mesh is employed to obtain the second-order interatomic force constants. **Fig. S11** shows the phonon dispersion relations obtained using 3×3×3 and 4×4×4 supercells with a *q*-point mesh of 1×1×1 for the RbCaAs and RbCaSb, which exhibited good consistency by the finite difference method, further demonstrating the computational reliability of this work.

3.2 Convergence tests of phonon transport property calculations

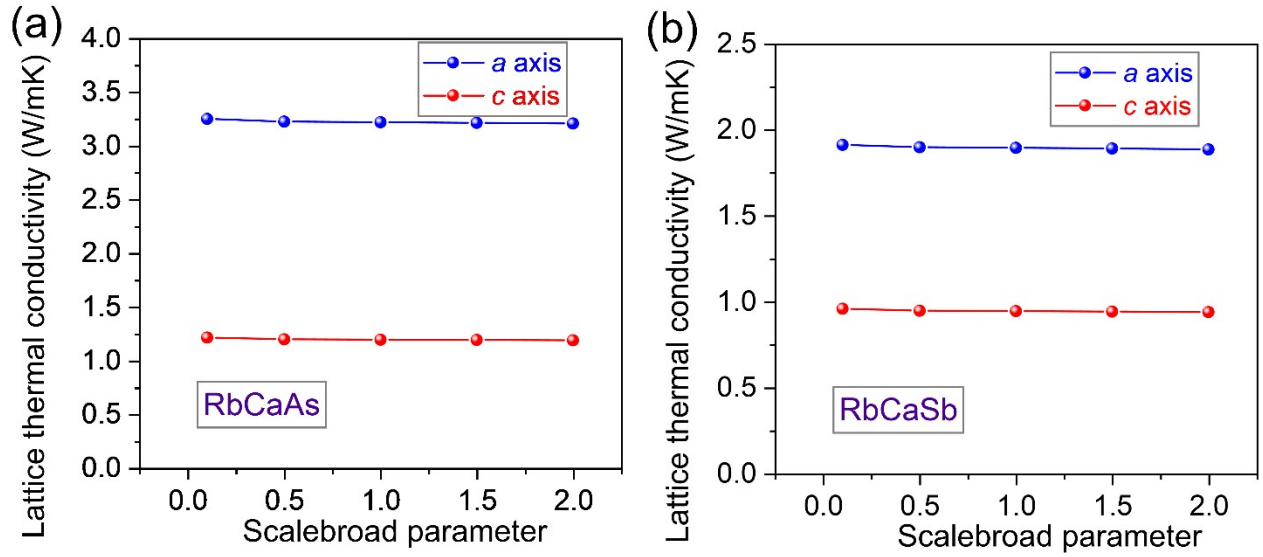

Fig. S12. Lattice thermal conductivity (K_l) at 300K as a function of scalebroad parameter for the (a) RbCaAs and (b) RbCaSb along the *a*-axis (blue dots) and *c*-axis (red dots). The Q-grid is set to 20×20×20, and the order of nearest neighbor atoms is set to 10^{th}.

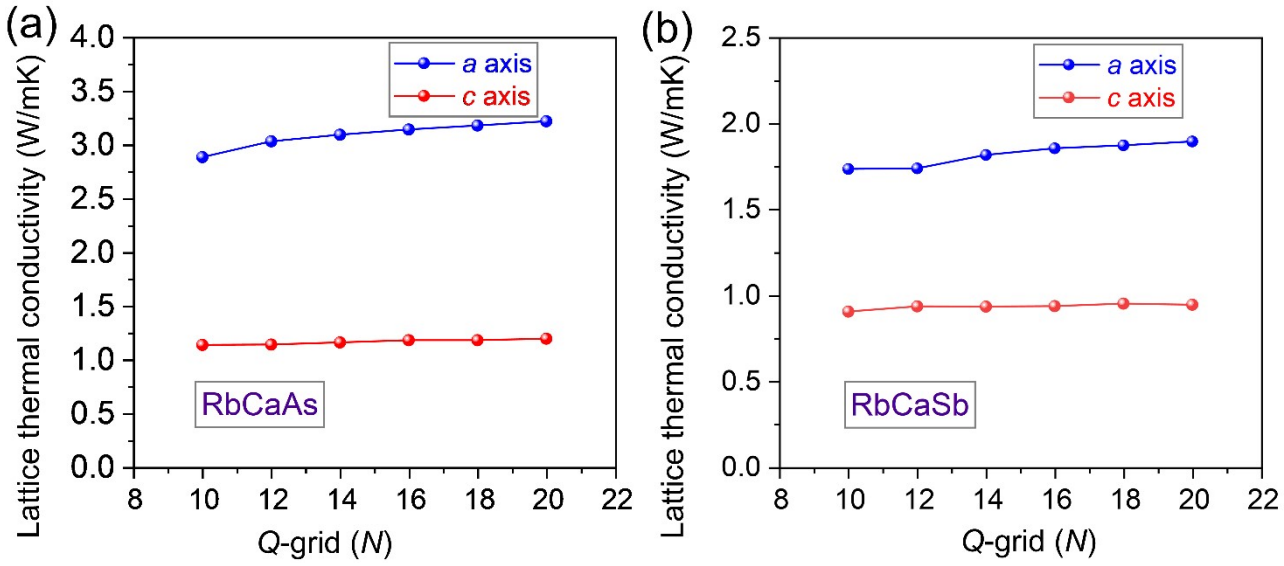

Fig. S13. Lattice thermal conductivity (K_l) at 300K as a function of Q-grid for the (a) RbCaAs and (b) RbCaSb along the *a*-axis (blue dots) and *c*-axis (red dots). The scalebroad parameter is set to 1.0, the order of nearest neighbor atoms is set to 10^{th}.

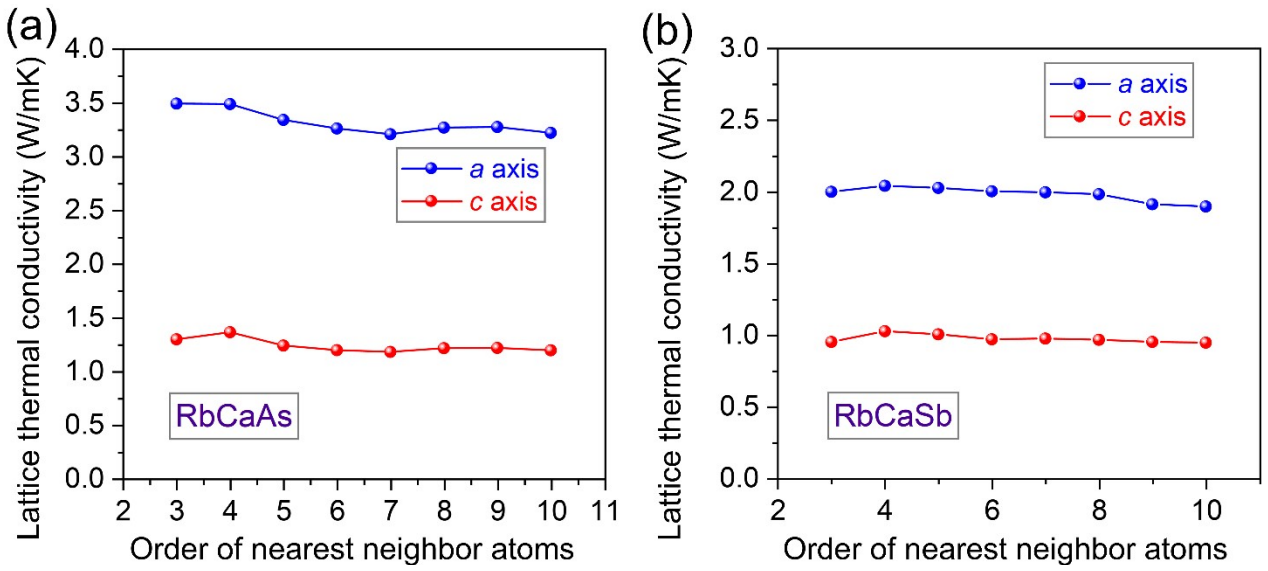

Fig. S14. Lattice thermal conductivity (K_l) at 300K as a function of different nearest neighbors of atoms for the (a) RbCaAs and (b) RbCaSb along the a-axis (blue dots) and *c*-axis (red dots). The scalebroad parameter is set to 1.0, The Q-grid is set to 20×20×20.

3.3 Thermal transport parameter calculations

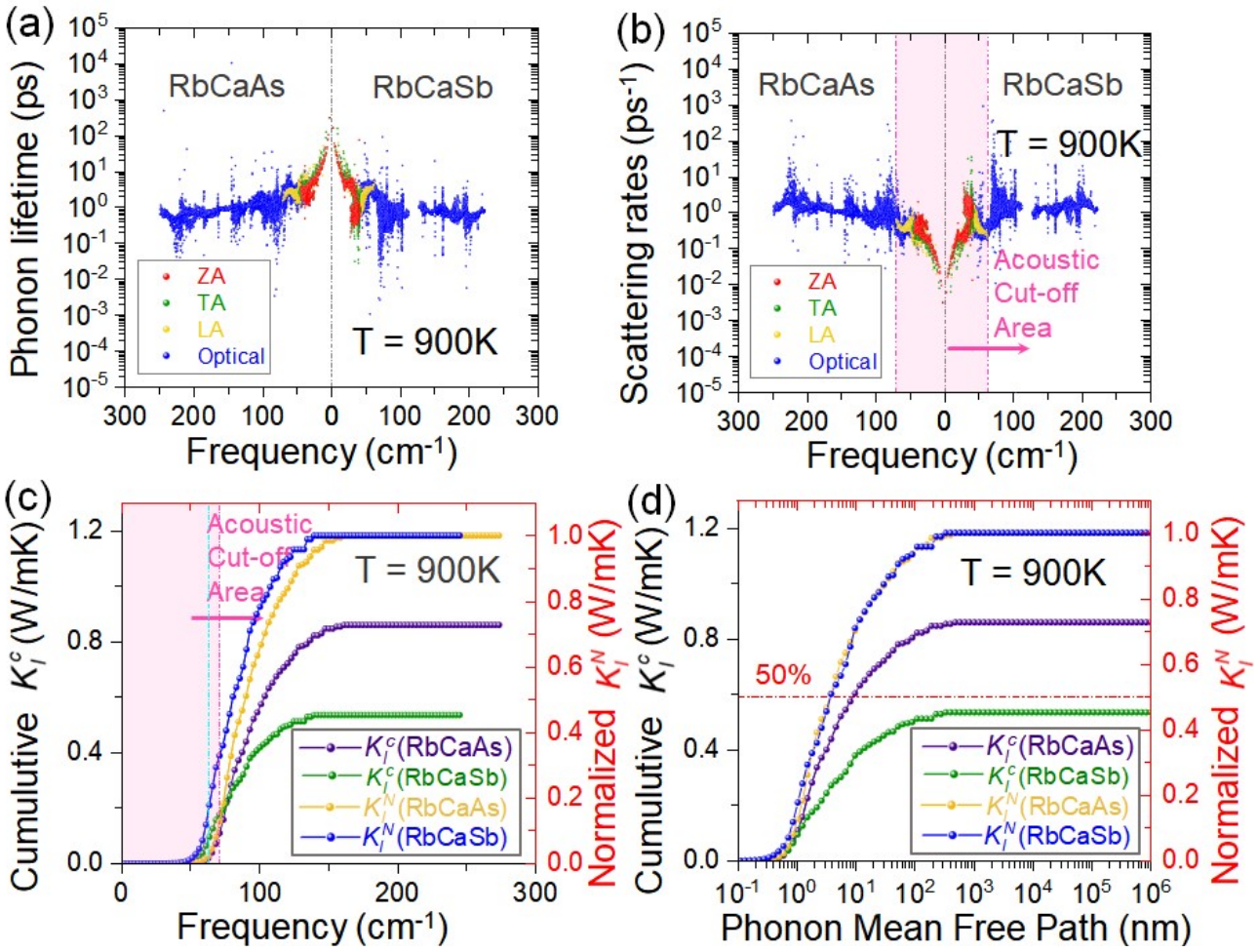

Fig. S15. Calculated (a) phonon lifetime and (b) scattering rates as a function of frequency at 900 K. (c) Cumulative and normalized lattice thermal conductivity (K_l^C and K_l^N) as a function of phonon frequency at 900 K for RbCaX (X = As, Sb). The pink area represents the acoustic cut-off. (d) Cumulative and normalized lattice thermal conductivity (K_l^C and K_l^N) as a function of phonon mean free path at 900 K for RbCaX (X = As, Sb). The red dashed line shows the thermal conductivity suppression to 50%.

References

1 Kresse G, Furthmüller J. Efficiency of ab-initio total energy calculations for metals and semiconductors using a plane-wave basis set. Comput Mater Sci, 1996, 6: 15-50